is described in the next theorem [19, 23, 31, 212, 233].

THEOREM 2.3 (Canards in $\mathbb{R}^3$). *For the slow-fast system* (2.14) *with $\varepsilon > 0$ sufficiently small the following holds:*

(C1) There are no maximal canards generated by a folded focus.

(C2) For a folded saddle the two singular canards $\tilde{\gamma}_{1,2}$ perturb to maximal canards $\gamma_{1,2}$.

(C3.1) For a folded node let $\mu := \sigma_w/\sigma_s < 1$. The singular canard $\tilde{\gamma}_s$ ("the strong canard") always perturbs to a maximal canard γ_s. If $\mu^{-1} \notin \mathbb{N}$ then the singular canard $\tilde{\gamma}_w$ ("the weak canard") also perturbs to a maximal canard γ_w. We call γ_s and γ_w primary canards.

(C3.2) For a folded node suppose $k > 0$ is an integer such that $2k + 1 < \mu^{-1} < 2k + 3$ and $\mu^{-1} \neq 2(k + 1)$. Then, in addition to $\gamma_{s,w}$, there are k other maximal canards, which we call secondary canards.

(C3.3) The primary weak canard of a folded node undergoes a transcritical bifurcation for odd $\mu^{-1} \in \mathbb{N}$ and a pitchfork bifurcation for even $\mu^{-1} \in \mathbb{N}$.

3. Slow-fast mechanisms for MMOs. In this section we present key theoretical results of how MMOs arise in slow-fast systems with SAOs occurring in a localized region of the phase space. The LAOs, on the other hand, are associated with large excursions away from the localized region of SAOs. More specifically, we discuss four local mechanisms that give rise to such SAOs:

- passage near a folded node, discussed in Section 3.1;
- singular Hopf bifurcation, discussed in Section 3.2;
- three-time-scale problems with a singular Hopf bifurcation, discussed in Section 3.3;
- tourbillion, discussed in Section 3.4.

Each of these local mechanisms has its distinctive characteristics and can give rise to MMOs when combined with a *global return mechanism* that takes the trajectory back to the region with SAOs. Such global return mechanisms arise naturally in models from applications and a classic example is an S-shaped slow manifold; see Section 3.2 and the examples in Sections 4–6. We do not discuss global returns in detail, but rather concentrate on the nature of the local mechanisms. From the analysis of normal forms we estimate quantities that can be measured in examples of MMOs produced from both numerical simulations and experimental data. Specifically, we consider the number of SAOs and the changes in their amplitudes from cycle to cycle. We also consider in model systems the geometry of nearby slow manifolds that are associated with the approach to and departure from the SAO regions.

3.1. MMOs due to a folded node. Folded nodes are only defined for the singular limit (2.4) of system (2.1) on the slow time scale. However, they are directly relevant to MMOs because for $\varepsilon > 0$ small enough, trajectories of (2.1) that flow through a region where the reduced system has a folded node, undergo small oscillations. Benoit [19, 20] first recognized these oscillations. Wechselberger and collaborators [31, 212, 233] gave a detailed analysis of folded nodes while Guckenheimer and Haiduc [86] and Guckenheimer [84] computed intersections of slow manifolds near a folded node and maps along trajectories passing through these regions. From Theorem 2.3 we know that the eigenvalue ratio $0 < \mu < 1$ at the folded node is a crucial quantity that determines the dynamics in a neighborhood of the folded node. In particular, μ controls the maximal number of oscillations. The studies mentioned above use normal forms to describe the dynamics of oscillations near a folded node. Two equivalent versions of these normal forms are

$$\begin{cases} \varepsilon\,\dot{x} &= y - x^2, \\ \dot{y} &= z - x, \\ \dot{z} &= -\nu, \end{cases} \qquad (3.1)$$

12

and

$$
\begin{cases}
\varepsilon\,\dot{x} &= y - x^2, \\
\dot{y} &= -(\mu + 1)x - z, \\
\dot{z} &= \tfrac{1}{2}\mu.
\end{cases}
\tag{3.2}
$$

Note that μ is the eigenvalue ratio of system (3.2) and that $\nu \neq 0$ and $\mu \neq 0$ imply that no equilibria exist in (3.1) and (3.2). If we replace (x, y, z) in system (3.1) by (u, v, w) and call the time variable τ_1, then we obtain system (3.2) via the coordinate change

$$
x = (1 + \mu)^{1/2}\, u, \quad y = (1 + \mu)\, v, \quad z = -(1 + \mu)^{3/2}\, w,
$$

and the rescaling of time $\tau = \tau_1/\sqrt{1 + \mu}$, which gives

$$
\nu = \frac{\mu}{2(1 + \mu)^2} \quad \text{or} \quad \mu = \frac{-1 + \sqrt{1 - 8\nu}}{-1 - \sqrt{1 - 8\nu}}.
$$

Therefore, in system (3.1) the number of secondary canards changes with the parameter ν. When ν is small, $\mu \approx 2\nu$. If the "standard" scaling [212] $x = \varepsilon^{1/2}\,\bar{x}$, $y = \varepsilon\,\bar{y}$, $z = \varepsilon^{1/2}\,\bar{z}$, and $t = \varepsilon^{1/2}\,\bar{t}$, is applied to system (3.1), we obtain

$$
\begin{cases}
\bar{x}' &= \bar{y} - \bar{x}^2, \\
\bar{y}' &= \bar{z} - \bar{x}, \\
\bar{z}' &= -\nu.
\end{cases}
\tag{3.3}
$$

Hence, the phase portraits of system (3.1) for different values of ε are topologically equivalent via linear maps. The normal form (3.3) describes the dynamics in the neighborhood of a folded node, which is at the origin here. Trajectories that come from $y = \infty$ with $x > 0$ and pass through the folded-node region make a number of oscillations in the process, before going off to $y = \infty$ with $x < 0$. There are no returns to the folded-node region in this system.

Let us first focus on the number of small oscillations. If $2k + 1 < \mu^{-1} < 2k + 3$, for some $k \in \mathbb{N}$, and $\mu^{-1} \neq 2(k + 1)$ then the primary strong canard γ_s twists once and the i-th secondary canard ξ_i, $1 \leq i \leq k$, twists $2i + 1$ times around the primary weak canard γ_w in an $O(1)$ neighborhood of the folded node singularity in system (3.3), which corresponds to an $O(\sqrt{\varepsilon})$ neighborhood in systems (3.1) and (3.2) [212, 233]. (A twist corresponds to a half rotation.) We illustrate this in Figure 6 for system (3.3) with $\nu = 0.025$. Note that $\nu = 0.025$ corresponds to $\mu \approx 0.0557$. Hence, $2k + 1 < \mu^{-1} \approx 17.953 < 2k + 3$ for $k = 8$, so Theorem 2.3 states that there exist eight secondary canards ξ_i, $1 \leq i \leq 8$, along with the strong and weak canards $\gamma_{s/w}$. Figure 6 shows the attracting slow manifold S_ε^a and the repelling slow manifold S_ε^r of (3.3) in a three-dimensional region bounded by the planes $\{z = \pm\alpha\}$, denoted Σ_α and $\Sigma_{-\alpha}$, with $\alpha = 0.14$; see Section 8 for details on how these computations were done. Even though the rescaled normal form (3.3) does not depend on ε anymore, we still indicate the ε-dependence of the slow manifolds to distinguish them from the attracting and repelling sheets of the critical manifold; furthermore, S_ε^a and S_ε^r can be thought of as the slow manifolds of (3.1) or (3.2). Both manifolds are extensions of Fenichel manifolds and illustrate how the slow manifolds intersect near the fold curve of the critical manifold; the fold curve is the z-axis. The intersection curves are the canard orbits; highlighted are the primary strong canard γ_s (black) and the first three secondary canards ξ_1 (orange), ξ_2 (magenta) and ξ_3 (cyan). The inset shows the intersection curves of S_ε^a and S_ε^r with the plane $\Sigma_{\mathrm{fn}} := \{z = 0\}$ that contains the folded node at the origin; the intersection points of the highlighted canard orbits are also indicated. Due to the symmetry of the normal
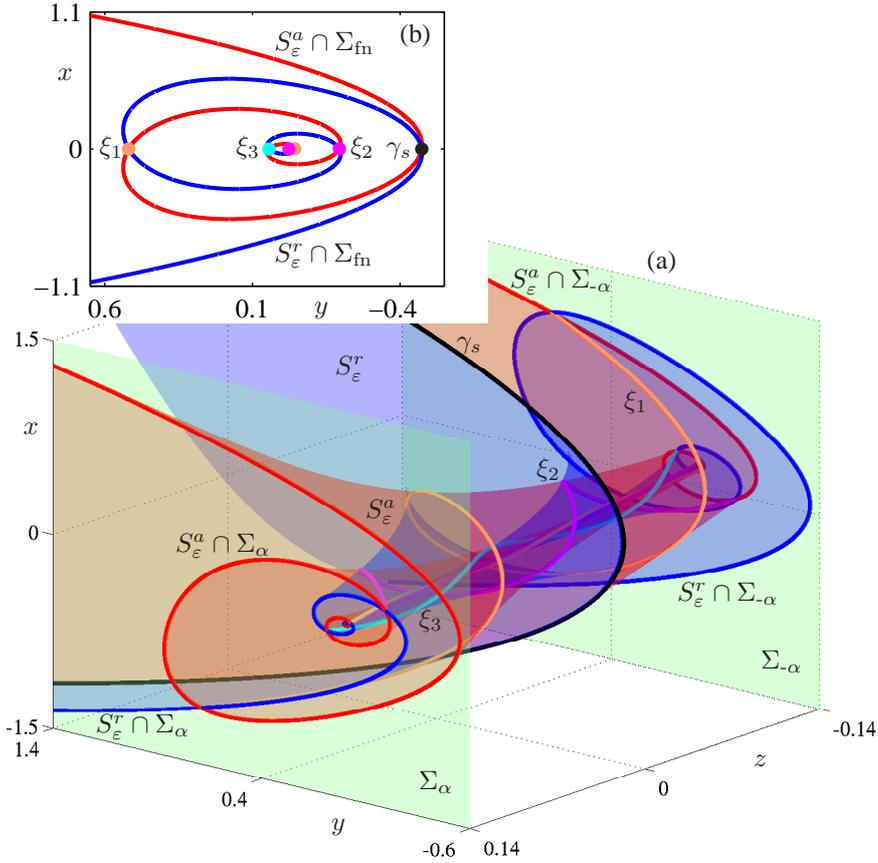
13

FIG. 6. *Invariant slow manifolds of (3.3) with $\nu = 0.025$ in a neighborhood of the folded node. Both the attracting slow manifold S_ε^a (red) and the repelling slow manifold S_ε^r (blue) are extensions of Fenichel manifolds. The primary strong canard γ_s (black curve) and three secondary canards ξ_1 (orange), ξ_2 (magenta) and ξ_3 (cyan) are the first four intersection curves of S_ε^a and S_ε^r; the inset shows how these objects intersect a cross-section orthogonal to the fold curve $\{x = 0, y = 0\}$.*

form (3.3), the two slow manifolds S_ε^a and S_ε^r are each other's image under rotation by π about the y-axis in Figure 6(a).

A trajectory entering the fold region becomes trapped in a region bounded by strips of S_ε^a and S_ε^r and two of their intersection curves. The intersection curves are maximal canards, and the trajectory is forced to follow the oscillations of these two bounding canard orbits. Figure 6 does not show very clearly how many canards there are, nor does it indicate the precise number of oscillations. We calculate the flow map of (3.3) with $\nu = 0.025$ to illustrate this better. Due to the strong contraction along S_ε^a, the flow map through the fold region is strongly contracting in one direction for trajectories that do not extend along S_ε^r. Hence, the flow map will be almost one dimensional and can be approximated by following trajectories starting on the critical manifold far away from the fold curve. Figure 7(a) shows the result of integrating 500 equally-spaced initial values on the line segment $\{x = 20, y = x^2 = 400, -3.25 \leq z \leq -0.75\}$ until they reach the plane $x = -10$; plotted are the z-coordinates of the final values versus the initial values. One can see ten segments in this flow map that are separated by discontinuities. These discontinuities mark sectors on the
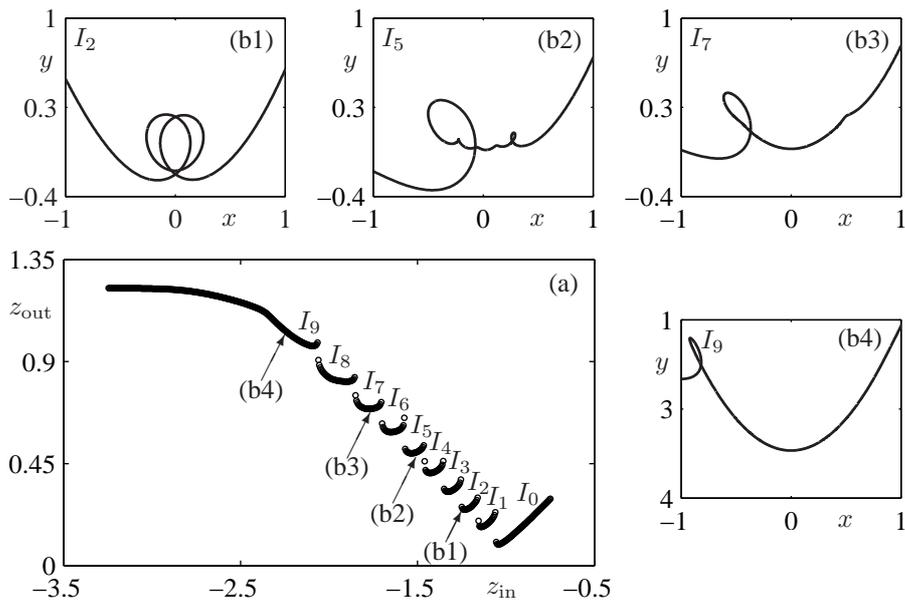
FIG. 7. *Numerical study of the number of rotational sectors for system* (3.3) *with* $\nu = 0.025$. *Panel (a) illustrates the flow map through the folded node by plotting the z-coordinates z_{out} of the first return to a cross-section $x = -10$ of 500 trajectories with equally-spaced initial values $(x, y, z) = (20, 400, z_{\text{in}})$, where $-3.25 \leq z_{\text{in}} \leq -0.75$. Panels (b1)–(b4) show four trajectories projected onto the (x, y)-plane that correspond to the points labeled in panel (c), where $z_{\text{in}} = -1.25$ in panel (b1), $z_{\text{in}} = -1.5$ in panel (b2), $z_{\text{in}} = -2$ in panel (b3), and $z_{\text{in}} = -2.25$ in panel (b4).*

line segment $\{x = 20, \; y = x^2 = 400, \; -3.25 \leq z \leq -0.75\}$ that correspond to an increasing number of SAOs; in fact, each segment corresponds to a two-dimensional sector $I_i, 0 \leq i \leq 9$, on the attracting sheet S_ε^a of the slow manifold. The outer sector I_0 on the right in Figure 7(a) is bounded on the left by the primary strong canard γ_s; sector I_1 is bounded by γ_s and the first maximal secondary canard ξ_1; sectors $I_i, i = 2, \ldots, 8$, are bounded by maximal secondary canard orbits ξ_{i-1} and ξ_i; and the last (left outer) sector I_9 is bounded on the right by ξ_8. On one side of the primary strong canard γ_s and each maximal secondary canard $\xi_i, 1 \leq i \leq 8$, trajectories follow the repelling slow manifold S_ε^r and then jump with decreasing values of x. On the other side of γ_s and ξ_i, trajectories jump back to the attracting slow manifold and make one more oscillation through the folded node region before flowing toward $x = -\infty$. The four panels (b1)–(b4) in Figure 7 show portions of four trajectories projected onto the (x, y)-plane; their initial values are $(x, y, z) = (20, 400, z_{\text{in}})$ with z_{in} as marked in panel (a), that is, $z_{\text{in}} = -1.25$, $z_{\text{in}} = -1.5$, $z_{\text{in}} = -2$ and $z_{\text{in}} = -2.25$ for (b1)–(b4), respectively. The trajectory in panel (b1) was chosen from the sector I_2, bounded by ξ_1 and ξ_2; this trajectory makes two oscillations. The trajectory in panel (b2) comes from I_5 and, indeed, it makes five oscillations. The other two trajectories, in panel (b3) and (b4), make seven and nine oscillations, respectively, but some of these oscillations are too small to be visible.

The actual widths of the rotational sectors in Figure 7 are very similar due to the ε-dependent rescaling used to obtain (3.3). When the equations depend on ε as in (3.1) and (3.2), however, the widths of the sectors depend on ε. In fact, every sector is very small except for the sector corresponding to maximal rotation, which is bounded by ξ_k and the fold curve. For an asymptotic analysis of the widths of the rotational sectors that organize the
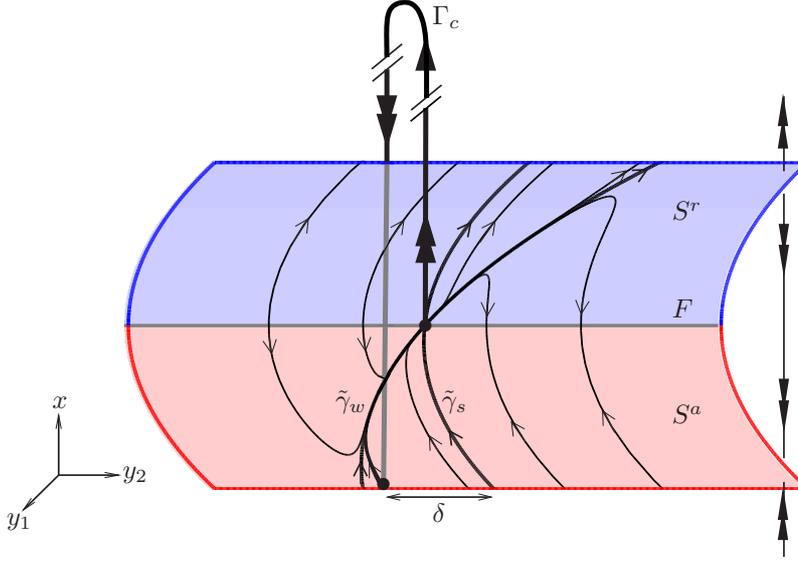
15

FIG. 8. *Schematic diagram of the candidate periodic orbit Γ_c that gives rise to MMOs with SAOs produced by a folded node singularity. The candidate Γ_c approaches the folded node along the attracting sheet S^a (red) of the critical manifold (red) in the sector of maximal rotation associated with the weak singular canard $\tilde{\gamma}_w$. The distance to the strong singular canard $\tilde{\gamma}_s$ is labeled δ. When the trajectory reaches the folded node (filled circle) it jumps along a layer and proceeds to make a global return.*

oscillations, system (3.2) is more convenient, because the eigenvalues of the desingularized slow flow are $-\mu$ and -1. Brøns, Krupa and Wechselberger [31] found the following.

THEOREM 3.1. *Consider system* (2.14) *and assume it has a folded node singularity. At an $O(1)$-distance from the fold curve, all secondary canards are in an $O(\varepsilon^{(1-\mu)/2})$-neighborhood of the primary strong canard. Hence, the widths of the rotational sectors I_i, $1 \le i \le k$, is $O(\varepsilon^{(1-\mu)/2})$ and the width of sector I_{k+1} is $O(1)$.*

Note that, as $\mu \to 0$ (the folded saddle-node limit), the number of rotational sectors increases indefinitely, and the upper bounds on their widths decrease to $O(\varepsilon^{1/2})$.

3.1.1. Folded node with a global return mechanism. A global return mechanism may reinject trajectories to the folded node funnel to create an MMO. Assuming that the return happens $O(1)$ away from the fold curve, Theorem 3.1 predicts the number of SAOs that follow. We create a candidate trajectory by following the fast flow starting at the folded node until it returns to the folded node region; this is sketched in Figure 8. The global return mechanism produces one LAO. Let δ denote the distance of the global return point of a trajectory from the singular strong canard $\tilde{\gamma}_s$ measured on a cross-section at a distance $O(1)$ away from the fold; we use the convention that $\delta > 0$ indicates a return into the funnel region. Provided δ is large enough, so that the global return point lands in the sector I_{k+1} of maximal rotation, one can show the existence of a *stable* MMO with signature 1^{k+1}, where k is determined by μ [31]. We summarize this existence result (in a more general setting) in the following theorem.

THEOREM 3.2 (Generic 1^{k+1} MMOs). *Consider system* (2.14) *with the following assumptions:*

(A0) *Assume that $0 < \epsilon \ll 1$ is sufficiently small, $\varepsilon^{1/2} \ll \mu$ and $k \in \mathbb{N}$ is such that $2k + 1 < \mu^{-1} < 2k + 3$.*

(A1) *The critical manifold S is (locally) a folded surface.*

16

(A2) The corresponding reduced problem possesses a folded node singularity.

(A3) There exists a candidate periodic orbit (as constructed in Figure 8) which consists of a segment on S^a (red) within the singular funnel (bounded by F and $\tilde{\gamma}_s$ such that it contains $\tilde{\gamma}_w$) with the folded node singularity as an endpoint, fast fibers of the layer problem and a global return segment.

(A4) A transversality hypothesis is satisfied that is not stated here because it is cumbersome to formulate precisely in a general setting; see e.g., [31] for the case of a cubic-shaped critical manifold.

Then there exists a stable MMO with signature 1^{k+1}.

Theorem 3.2 not only requires sufficiently small $0 < \varepsilon \ll 1$ but also $\mu \gg \varepsilon^{1/2}$ (while $0 < \mu < 1$). However, ε is usually of the order $O(10^{-2})$ in applications, so that μ must be close to 1 in order for the theorem to apply. Therefore, such maximal MMO signatures are seldom seen in applications. Furthermore, the SAOs for an MMO with signature 1^{k+1} tend to be too small to be readily visible.

Figure 7 illustrates that the amplitudes of the SAOs are much larger for trajectories that approach the folded node close to the strong canard and lie in one of the sectors I_i with $i \leq k$ rather than I_{k+1}. We know from Theorem 3.1 that the maximal width of a sector I_i with $i \leq k$ is bounded from above by $O(\varepsilon^{(1-\mu)/2})$ with $\mu < 1/3$. When δ is $O(\varepsilon^{(1-\mu)/2})$ one can, indeed, find MMOs with $i \leq k$ SAOs that are stable. Geometrically, different stable MMOs are selected as one moves the flow map in Figure 7(a) up or down; since the rotational sector I_{k+1} for general ε-dependent systems has much larger width than the other sectors, one should expect that the transitions through I_i with $i \leq k$ happen rather quickly during a parameter-induced variation of δ. We have the following result [31].

THEOREM 3.3. *Suppose system* (2.14) *satisfies assumptions (A0)–(A3) of Theorem 3.2 and additionally:*

(A5) For $\delta = 0$, the global return point is on the singular strong canard $\tilde{\gamma}_s$ and as δ passes through zero the return point crosses $\tilde{\gamma}_s$ with nonzero speed.

Suppose now that $\delta = O(\varepsilon^{(1-\mu)/2}) > 0$. Then, for sufficiently small $0 < \varepsilon \ll 1$ and $k \in \mathbb{N}$ such that $2k + 1 < \mu^{-1} < 2k + 3$ the following holds. For each i, $1 \leq i \leq k$, there exist subsectors $\tilde{I}_i \subset I_i$ with corresponding distance intervals (δ_i^-, δ_i^+) of widths $O(\varepsilon^{(1-\mu)/2})$, which have the property that if $\delta \in (\delta_i^-, \delta_i^+)$ then there exists a stable MMO with signature 1^i.

Theorem 3.3 says that we should observe a succession of stable 1^i MMOs with increasingly more SAOs as δ increases (assuming that μ remains fixed in such a parameter variation). In the transition from a 1^i to a 1^{i+1} MMO signature, that is, in the regions in between intervals (δ_i^-, δ_i^+) and $(\delta_{i+1}^-, \delta_{i+1}^+)$ we expect to find more complicated signatures, which are usually a mix of 1^i and 1^{i+1}. As with Theorem 3.2, the amplitudes of most SAOs will be tiny if ε is small, except for those MMOs that have only a few SAOs after each LAO.

If $\mu = O(\varepsilon^{1/2})$, that is, assumption (A0) does not hold, then we may still expect stable MMO signatures of type 1^{k+1}, as soon as the global returns falls inside the funnel region and $\delta = O(1)$ [143]; note that $k = O(1/\varepsilon^{1/2})$ and the amplitudes of the SAOs for such an MMO will again be tiny. If $\mu = O(\varepsilon^{1/2})$ and $\delta = O(\varepsilon^{1/2})$ as well, the mixed MMO signatures with larger-amplitude SAOs are more likely to occur. For example, Figure 20 in Section 4 displays an MMO of type $1^2 1^3$ in the Koper model. Here, global returns come very close to the secondary maximal canard ξ_2, first slightly to the left (hence, into the rotational sector I_2 with two SAOs) and then slightly to the right (hence, into the rotational sector I_3 with three SAOs), creating this MMO signature.

The theory described so far does not capture all of the possible dynamics near a folded node. If higher-order terms are included in the normal forms (3.1)-(3.2), then equilibria may

appear in an $O(\varepsilon^{1/2})$ neighborhood of the folded node as soon as $\mu = O(\varepsilon^{1/2})$ or smaller. This observation motivates our study of the singular Hopf bifurcation in three dimensions.

3.2. MMOs due to a singular Hopf bifurcation. Equilibria of a slow-fast system (2.1) always satisfy $f(x, y, \lambda, \varepsilon) = 0$; generically, they are located in regions where the associated critical manifold S is normally hyperbolic. However, in generic one-parameter families of slow-fast systems, the equilibrium may cross a fold of S. In generic families with two slow variables, the fold point (including the specific parameter value) at which the equilibrium crosses the fold curve of the critical manifold has been called a *folded saddle-node of type II* [161]. Folded nodes and saddles of the reduced system are not projections of equilibria of the full slow-fast system, but the folded saddle-nodes of type II are. When $\varepsilon > 0$, the system has a singular Hopf bifurcation, which occurs generically at a distance $O(\varepsilon)$ in parameter space from the folded saddle-node of type II [85].

In order to obtain a normal form for the singular Hopf bifurcation, we follow [85] and add higher-order terms to the normal form (3.1) of the folded node, to obtain

$$\begin{cases} \varepsilon \dot{x} &= y - x^2, \\ \dot{y} &= z - x, \\ \dot{z} &= -\nu - a\,x - b\,y - c\,z. \end{cases} \tag{3.4}$$

As with (3.1), we apply the standard scaling [212] $x = \varepsilon^{1/2}\,\bar{x}$, $y = \varepsilon\,\bar{y}$, $z = \varepsilon^{1/2}\,\bar{z}$, and $t = \varepsilon^{1/2}\,\bar{t}$; system (3.4) then becomes

$$\begin{cases} \bar{x}' &= \bar{y} - \bar{x}^2, \\ \bar{y}' &= \bar{z} - \bar{x}, \\ \bar{z}' &= -\nu - \varepsilon^{1/2}\,a\,\bar{x} - \varepsilon\,b\,\bar{y} - \varepsilon^{1/2}\,c\,\bar{z}. \end{cases} \tag{3.5}$$

This scaled vector field provides an $O(\varepsilon^{1/2})$-zoom of the neighborhood of the folded singularity where SAOs are expected to occur. The scaling removes ε from the first equations while the coefficients a, b and c of the third equation become ε-dependent; ν remains fixed. Note that the coefficient of $\bar{y}$ tends to 0 faster than those of $\bar{x}, \bar{z}$ as $\varepsilon \to 0$. This feature makes the definition of normal forms for slow-fast systems somewhat problematic: scalings of the state-space variables and the singular perturbation parameter ε interact with each other. These ε-dependent scalings play an important role in "blow-up" analysis of fold points and folded singularities.

In contrast to the normal form (3.1) of a folded node, system (3.5) possesses equilibria for all values of ν. If $\nu = O(1)$ then these equilibria are far from the origin, with coordinates that are $O(\varepsilon^{-1/2})$ or larger. Since we want to study the dynamics near a folded singularity, the ε-dependent terms in (3.5) play little role in this parameter regime and the system can be regarded as an inconsequential perturbation of the folded node normal form (3.3) and Theorems 3.2 and 3.3 apply. On the other hand, if $\nu = O(\varepsilon^{1/2})$ or smaller then one equilibrium lies within an $O(1)$-size domain of the phase space. This equilibrium is determined by the coefficients a and c (to leading order) and plays an important role in the local dynamics near a folded singularity [85, 143]. In particular, the equilibrium undergoes a singular Hopf bifurcation for $\nu = O(\varepsilon)$ [85]. Thus, for parameter values $\nu = O(\varepsilon^{1/2})$ or smaller, the higher-order terms in the third equation of (3.5) are crucial.

So what is the most appropriate normal form of a system that undergoes a singular Hopf bifurcation? Several groups have derived system (3.4), but drop the term by because it has higher order in ε after the scaling. However, this term appears in the formula for the lowest-order term in ε of the first Lyapunov coefficient of the Hopf bifurcation of (3.4) and, hence,
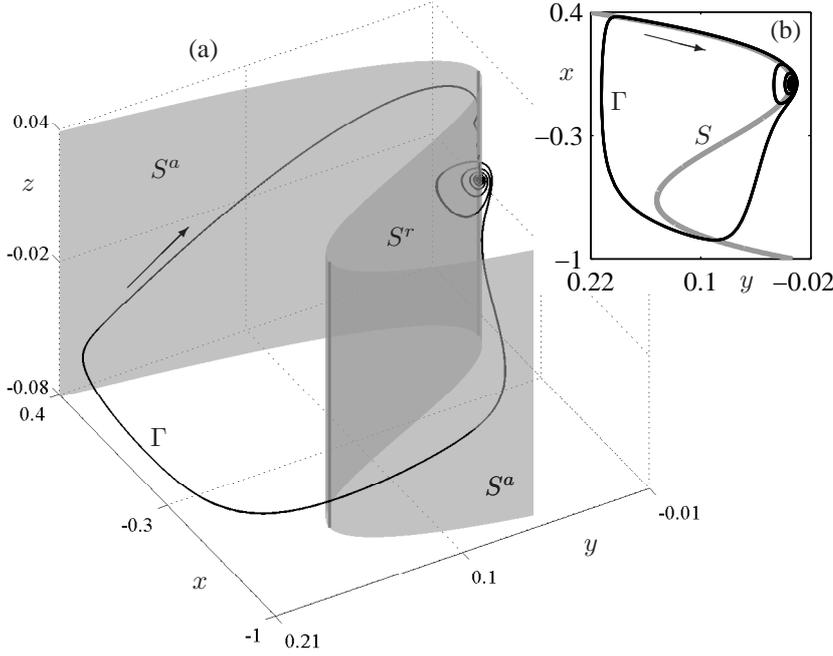
FIG. 9. *Phase portrait of an MMO periodic orbit* Γ *(black curve) for system* (3.6) *with* $(\nu, a, b, c, \varepsilon) = (0.0072168, -0.3872, -0.3251, 1.17, 0.01)$. *The critical manifold S (grey) is the S-shaped surface with folds at $x = 0$ and $x = -\frac{2}{3}$. The orbit Γ is composed of two slow segments near the two attracting sheets of S and two fast segments, with SAOs in the region near the equilibrium p on the repelling sheet S^r of S just past the fold at $x = 0$. Panel (a) shows a three-dimensional view and panel (b) the projection onto the (x, y)-plane.*

must be retained if we hope to determine a complete unfolding of the singular Hopf bifurcation [85].

The MMOs that occur close to the singular Hopf bifurcation have a somewhat different character than those generated via the folded node mechanism. Guckenheimer and Willms [93] observed that a subcritical (ordinary) Hopf bifurcation may result in large regions of the parameter space being funneled into a small neighborhood of a saddle equilibrium with unstable complex eigenvalues. After trajectories come close to the equilibrium, SAOs grow in magnitude as the trajectory spirals away from the equilibrium. Similar MMOs may pass near a singular Hopf bifurcation. Then the equilibrium is a saddle-focus and trajectories on the attracting Fenichel manifold are funneled into a region close to the one-dimensional stable manifold of the equilibrium. SAOs occur as the trajectory spirals away from the equilibrium. We review here our incomplete understanding of singular Hopf bifurcations and the MMOs passing nearby.

The normal form (3.4) does not yield MMOs because there is no global return mechanism; trajectories that leave the vicinity of the equilibrium point and the fold curve flow to infinity in finite time. This property can be changed by adding a cubic term to the normal form that makes the critical manifold S-shaped, similar to the Van der Pol equation:

$$\begin{cases} \varepsilon \, \dot{x} &= y - x^2 - x^3, \\ \dot{y} &= z - x, \\ \dot{z} &= -\nu - a\,x - b\,y - c\,z. \end{cases} \qquad (3.6)$$

This version of the normal form for singular Hopf bifurcation with global reinjection has been
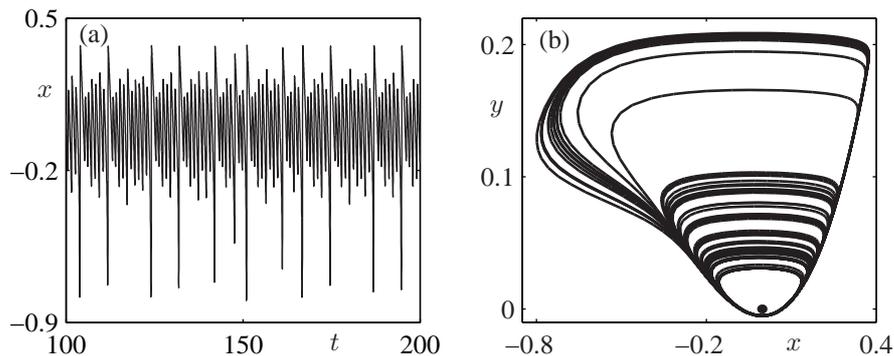
FIG. 10. A chaotic MMO trajectory of system (3.6) with $(\nu, a, b, c, \varepsilon) = (0.004564, -0.2317, 0.2053, 1.17, 0.01)$. Panel (a) shows the time series of the x-coordinate of the trajectory from $t = 100$ to $t = 200$, and panel (b) the projection of the trajectory onto the (x, y)-plane.

derived repeatedly as a "reduced" model for MMOs [122, 138]. An example of the overall structure of MMOs in system (3.6) with small ν is shown in Figure 9 for $(\nu, a, b, c, \varepsilon) = (0.0072168, -0.3872, -0.3251, 1.17, 0.01)$; note that $\nu = O(\varepsilon)$. The S-shaped critical manifold S is the grey surface in Figure 9(a); a top view is shown in panel (b). The manifold S has two fold curves, one at $x = 0$ and one at $x = -\frac{2}{3}$, that decompose S into one repelling and two attracting sheets. For our choice of parameters there exists a saddle-focus equilibrium p on the repelling sheet that is close to the origin (which is the folded node singularity). The equilibrium p has a pair of unstable complex conjugate eigenvalues. A stable MMO periodic orbit Γ, shown as the black curve in Figure 9, interacts with p as follows. Starting just past the fold at $x = 0$, that is, in the region near the origin with $x < 0$, the orbit Γ spirals away from p along its two-dimensional unstable manifold and repeatedly intersects the repelling sheet S^r of S. As soon as Γ intersects the repelling slow manifold (not shown), it jumps to the attracting sheet of S with $x < -\frac{2}{3}$. The orbit Γ then follows this sheet to the fold at $x = -\frac{2}{3}$, after which it jumps to the attracting sheet of S with $x > 0$. Then Γ returns to the neighborhood of p and the periodic motion repeats.

The MMO periodic orbit Γ displayed in Figure 9 is only one of many types of complex dynamics present in system (3.6). One aspect of the complex dynamics in system (3.6) is the fate of the periodic orbits created in the Hopf bifurcation. There are parameter regimes for (3.6) with stable periodic orbits of small amplitude created by a supercritical Hopf bifurcation. Subsequent bifurcations of these periodic orbits may be period-doubling or torus bifurcations [85]. Period-doubling cascades can give rise to small-amplitude chaotic invariant sets that may be associated with chaotic MMOs. For example, Figure 10 plots a chaotic MMO trajectory for (3.6) with $(\nu, a, b, c, \varepsilon) = (0.004564, -0.2317, 0.2053, 1.17, 0.01)$ that arises from such a period-doubling cascade of the periodic orbit emerging from the singular Hopf bifurcation. It appears that it is chaotic because of the nonperiodicity of its time series, shown for the x-coordinate in Figure 10(a). A two-dimensional projection onto the (x, y)-plane is shown in panel (b). Note that this trajectory does not come close to either the equilibrium point p or the folded singularity at the origin. As ν decreases from the value used in Figure 10 (where ν is already of order $O(\varepsilon)$), the large-amplitude epochs of the trajectories become less frequent and soon disappear, resulting in a small-amplitude chaotic attractor. Section 4 discusses a rescaled subfamily of (3.6), giving further examples of complex dynamics and some analysis of the organization of MMOs associated with this system.

We would like to characterize the parameter regimes with MMOs for which the SAOs
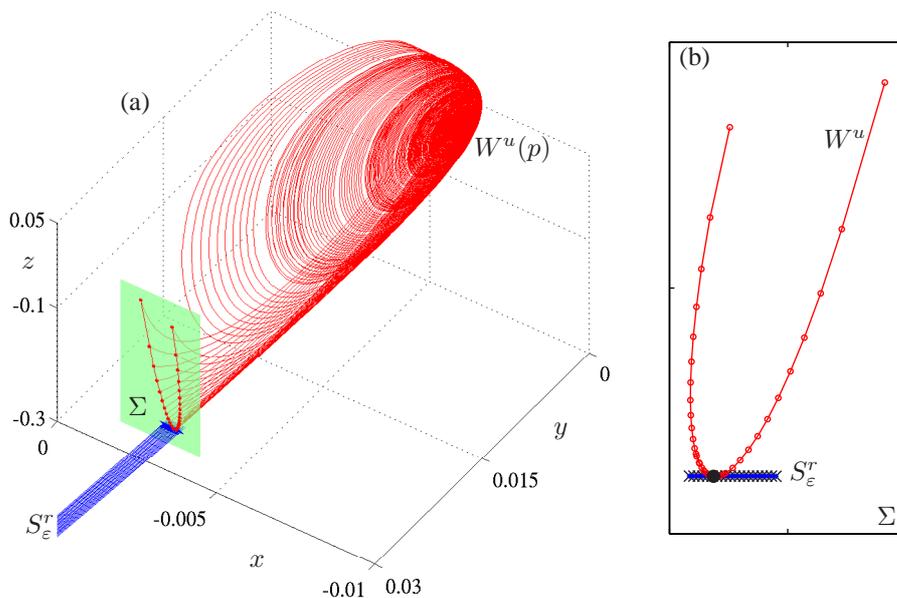
FIG. 11. *Tangency between the unstable manifold $W^u(p)$ of the equilibrium and the repelling slow manifold S^r_ε of (3.6) with $(\nu, a, b, c, \varepsilon) = (0.007057, 0.008870, -0.5045, 1.17, 0.01)$. Panel (a) shows trajectories of $W^u(p)$ (red) and S^r_ε (blue) that are terminated on the green cross-section Σ defined by $y = 0.3$. The intersections $W^u(p) \cap \Sigma$ (with points on computed trajectories marked 'o') and $S^r_\varepsilon \cap \Sigma$ (with points on computed trajectories marked 'x') are shown in panel (b).*

are solely or partially due to spiraling along the unstable manifold $W^u(p)$ of a saddle-focus p. Analysis of this issue appears to be significantly more complicated than that for folded nodes and has barely begun. We offer a few insights in locating these parameter regimes. First, we think of ν in the normal form (3.6) of the singular Hopf bifurcation as the "primary" bifurcation parameter and seek ranges of ν where MMOs are found. If the Hopf bifurcation at $\nu = \nu_H$ is supercritical then, for parameters close enough to the Hopf bifurcation, the limit set of $W^u(p)$ is just the bifurcating stable periodic orbit. The onset of MMOs is observed to occur at a distance $\nu = O(\varepsilon)$ from the Hopf bifurcation due to a new type of bifurcation [85]. This bifurcation occurs at parameters where p is a saddle-focus and $W^u(p)$ is tangent to the two-dimensional repelling Fenichel manifold S^r_ε. At first glance one might think that two unstable objects in a dynamical system cannot intersect. However, recall that $W^u(p)$ consists of trajectories that approach p as $t \to -\infty$ while S^r_ε consists of forward trajectories that remain slow for an $O(1)$ time on the slow time scale. Consequently, it is possible for a single trajectory to satisfy the criteria to belong to both of these objects. Figure 11 illustrates an example of a tangency between $W^u(p)$ and S^r_ε for (3.6) with $(\nu, a, b, c, \varepsilon) = (0.007057, 0.008870, -0.5045, 1.17, 0.01)$ (note that $\nu = O(\varepsilon)$ and, hence, very close to $\nu_H \approx -8.587 \times 10^{-5}$). Shown are a collection of trajectories on $W^u(p)$ (red) that start close to p and end in the cross-section $\Sigma := \{y = 0.3\}$, together with a collection of trajectories on S^r_ε that start on the repelling sheet of the critical manifold and also end in Σ; see Section 8.1 for details of the method used to compute these manifolds. Figure 11(b) shows the tangency of the two intersection curves of $W^u(p)$ and S^r_ε with Σ. The manifold S^r_ε is a surface that separates trajectories that make large-amplitude excursions from ones that remain in the vicinity of p. For values of ν such that $W^u(p)$ and S^r_ε do not intersect, the limit set of $W^u(p)$ remains small. By varying ν such that we move further away from ν_H, the

21

MMOs arise as soon as $W^u(p)$ and S_ε^r begin to intersect; see also Section 4.

The number of SAOs that an MMO periodic orbit Γ makes along $W^u(p)$ is determined by how close Γ comes to p and by the ratio of real to imaginary parts of the complex eigenvalues of p. The only way to approach p is along its stable manifold $W^s(p)$, so an MMO like that displayed in Figure 9 must come very close to $W^s(p)$. The minimum distance d between an MMO and $W^s(p)$ is analogous to the distance δ of a trajectory from the primary strong canard in the case of folded nodes. Unlike the case of a folded node, the maximal amplitude of the SAOs observed near $W^u(p)$ is largely independent of d. What does change as $d \to 0$ is that the epoch of SAOs increases in length and begins with oscillations that are too small to be detectable. There has been little investigation of how the parameters of the normal form (3.6) influence d, but Figure 8 in Guckenheimer [85] illustrates that d depends upon the parameter c in a complex manner. There are parameter regions where the global returns of MMO trajectories are funneled close to $W^s(p)$. Since MMOs are not found immediately adjacent to supercritical Hopf bifurcations, the ratio of real to imaginary parts of the complex eigenvalues remains bounded away from 0 on MMO trajectories. This prevents the appearance of extraordinarily long transients with oscillations that grow arbitrarily slowly like those found near a subcritical Hopf bifurcation; see Section 5 and also [87, Figure 5].

The singular-Hopf and folded-node mechanisms for creating SAOs are not mutually exclusive and can be present in a single MMO in the transition regime with $\nu = O(\varepsilon^{1/2})$. The specific behavior that one finds depends in part on whether the equilibrium p near the singular Hopf bifurcation is a saddle-focus with a pair of complex eigenvalues or a saddle with two real eigenvalues. The MMO displayed in Figure 21 contains some SAOs that lie inside the rotational sectors between the attracting and repelling slow manifolds and some SAOs that follow the unstable manifold of the saddle-focus equilibrium. On the other hand, we note that SAOs cannot be associated with a saddle equilibrium that has only real eigenvalues; this occurs in a parameter region with $\nu > (a + c)\varepsilon^{1/2}$ (to leading order), but $\nu = O(\varepsilon^{1/2})$. In this case, SAOs are solely associated with the folded node-type mechanism described for $\nu = O(1)$ (that is, $\mu = O(1)$). Krupa and Wechselberger [143] analyzed the transition regime $\nu = O(\varepsilon^{1/2})$ and showed that the folded node theory can be extended into this parameter regime provided the global return mechanism projects into the funnel region.

3.3. MMOs in three-time-scale systems. When the coefficients ν, a, b and c in the normal forms (3.4) and (3.6) of the singular Hopf bifurcation are of order $O(\varepsilon)$ or smaller, then z evolves slowly relative to y and the system actually has three time scales: fast, slow and super slow. Krupa et al. [138] studied this regime with geometric methods and asymptotic expansions for the case $a = c = 0$. They observed MMOs for which the amplitudes of the SAOs remain relatively large. Their analysis is based upon rescaling the system such that it has two fast variables and one slow variable. To make the three-time-scale structure explicit, we set $\nu = \varepsilon\hat{\nu}$, $a = \varepsilon\hat{a}$, $b = \varepsilon\hat{b}$ and $c = \varepsilon\hat{c}$. Rescaling the singular-Hopf normal form (3.6) of Section 3.2 by $x = \varepsilon^{1/2}\,\bar{x}$, $y = \varepsilon\,\bar{y}$, $z = \varepsilon^{1/2}\,\bar{z}$, and $t = \varepsilon^{1/2}\,\bar{t}$ yields

$$\begin{cases} \dot{x} &= y - x^2 - \varepsilon^{1/2}x^3, \\ \dot{y} &= z - x, \\ \dot{z} &= \varepsilon(-\hat{\nu} - \varepsilon^{1/2}\,\hat{a}\,x - \varepsilon\,\hat{b}\,y - \varepsilon^{1/2}\,\hat{c}\,z), \end{cases} \quad (3.7)$$

which is still a singularly perturbed system, but now with two fast variables, x and y, and a slow variable z. An equilibrium lies within an $O(1)$-size domain around the origin if $\hat{\nu} = O(\varepsilon^{1/2})$ or smaller, i.e., $\nu = O(\varepsilon^{3/2})$ or smaller. This equilibrium plays an important role in the dynamics if it is of saddle-focus type. In particular, it undergoes a Hopf bifurcation for $\hat{\nu} = O(\varepsilon)$, i.e., $\nu = O(\varepsilon^2)$.
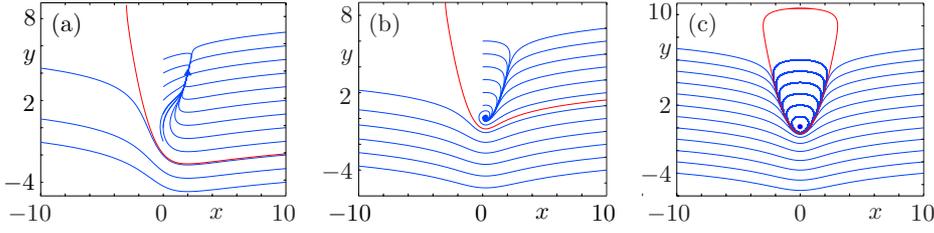
FIG. 12. *Phase portraits of system* (3.8) *for three different values of z. Shown are several trajectories (blue) and one trajectory (red) that approximates a separatrix. For each z, there is a single equilibrium point p at* $(x, y) = (z, z^2)$*. Panels (a)–(c) are for z = 2, z = 0.25 and z = 0, for which p is a stable node, a stable focus and a center surrounded by a continuous family of periodic orbits, respectively. The boundary of this family is the maximal canard.*

The two-dimensional layer problem of (3.7)

$$\begin{cases} \dot{x} &= y - x^2, \\ \dot{y} &= z - x, \\ \dot{z} &= 0, \end{cases} \qquad (3.8)$$

in which z acts as a parameter, is exactly the same system obtained in the analysis of the planar canard problem, where the parameter λ is replaced by z; compare with system (2.7).

Note that (3.8) has a unique equilibrium p for each value of z, given by $(x, y) = (z, z^2)$. Figure 12 shows phase portraits of (3.8) in the (x, y)-plane for three different values of z, namely $z = 2$, $z = 0.25$ and $z = 0$ in panels (a), (b) and (c), respectively. For $z > 0$, the equilibrium p is an attracting fixed point in the (x, y)-plane; it is a node for $z > 1$ and a focus for $0 < z < 1$; note that this information also determines the type of equilibrium of (3.7) obtained for $\hat{\nu} = O(\varepsilon^{1/2})$ to leading order — the same argument can also be used to determine the basin boundary of the saddle-focus equilibrium in Section 3.2. The basin boundary of p is an unbounded trajectory that is shown in red in panels (a) and (b). When $z = 0$, the vector field (3.8) has a time-reversing symmetry that induces the existence of a family of periodic orbits. Indeed, the function $H(x, y) = \exp(-2y)(y - x^2 + \frac{1}{2})$ is an integral of the motion and the level curve $H = 0$ is a parabola that separates periodic orbits surrounding p (the origin) from unbounded orbits that lie below the parabola and become unbounded with $x \to \pm\infty$ in finite time.

System (3.7) can be viewed as a perturbation of (3.8) when z remains small and is slowly varying compared to x and y. In this case, changes in H can be used to monitor the SAOs of trajectories. We focus on the case $a = c = 0$ studied in [138]. To find parameters for which system (3.6) has MMOs, we fix $b = -0.005$ and $\varepsilon = 0.01$ and vary ν so that z increases when y is large but decreases when the system has SAOs. More precisely, we want the average value of z to increase during epochs of SAOs and decrease during epochs of LAOs. The changes in z should be of sufficient magnitude to drive the trajectory across the slow manifolds and trigger a transition between these epochs. Figure 13(a) displays a periodic MMO with signature 1^4 found at $\nu = 0.00015$ (which is of order $O(\varepsilon^2)$). The projection in panel (a2) of the orbit onto the (z, y)-plane shows that z decreases approximately from -0.003713 to -0.004143 while the trajectory makes four SAOs, and z increases during a single LAO. Note that $\dot{z} = 0$ on the plane $y = 0.03$. System (3.6) also possesses two equilibria with z-coordinates given by $\pm\sqrt{-\nu/(b\varepsilon)}$, which equals $\pm\sqrt{3}$ in this case. Since the MMO signature shown in Figure 13(a2) is confined to the area near the origin (in the z-direction), these two equilibria have no influence on the dynamics.

As ν increases, the value of y for which $\dot{z} = 0$ increases, and trajectories have a
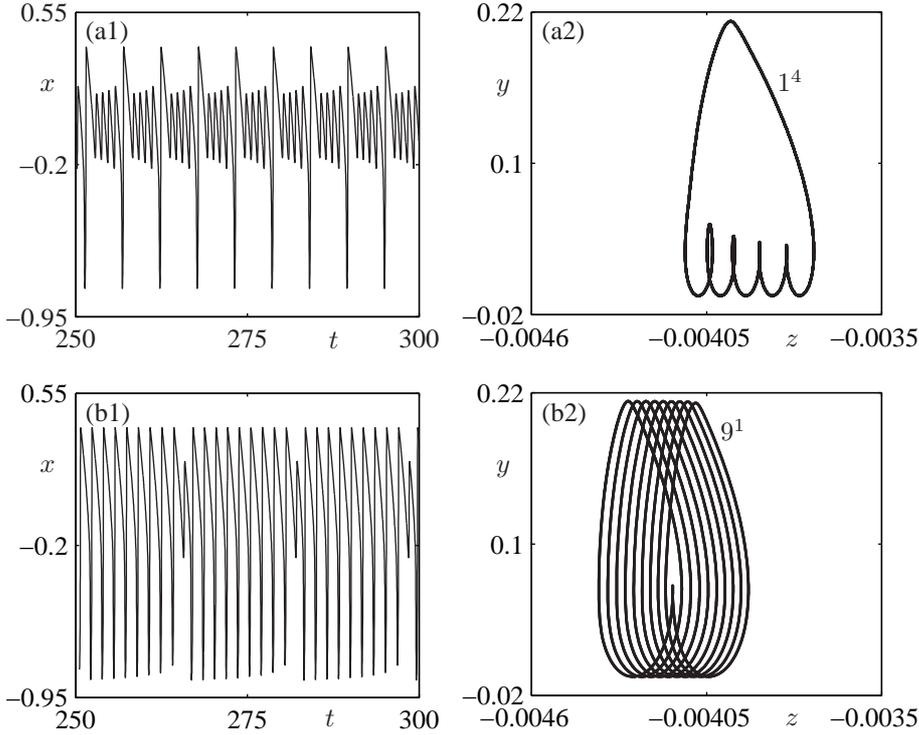
FIG. 13. *Stable periodic MMOs of system (3.6) with $(a, b, c, \varepsilon) = (0, -0.005, 0, 0.01)$. Row (a) shows the periodic MMO with signature 1^4 for $\nu = 0.00015$ as a time series of x in panel (a1) and in projection onto the (z, y)-plane in panel (a2); similar projections are shown in row (b) for $\nu = 0.00032$, where the periodic MMO has signature 9^1.*

propensity to pass more quickly through the region of SAOs. Figure 13(b) shows a periodic MMO with signature 9^1 obtained for $\nu = 0.00032$. This value of ν lies close to the upper end of the range in which MMOs seem to exist for the chosen values of $(a, b, c, \varepsilon) = (0, -0.005, 0, 0.01)$. As the projection in panel (b2) illustrates, the average value of z increases ($|z|$ decreases) during each LAO, but it takes nine LAOs before it crosses the threshold into the region of SAOs. On the other hand, a single SAO takes the trajectory back to the region of LAOs.

For intermediate values of $\nu \in (0.00015, 0.00032)$, the system displays aperiodic MMOs as well as periodic MMOs with a variety of signatures. These signatures can be analyzed via an approximately one-dimensional return map to a cross-section at $x = 0$. Returns to this cross-section with x decreasing appear to lie along a thin strip; this is illustrated in Figure 14(a) for $\nu = 0.0003$, for which the system appears to have aperiodic MMOs. The thin strip in Figure 14(a) is approximately given by the line $y = 0.1153\,z - 0.004626$ (and $x = 0$). If we take 600 initial conditions on this line with $z \in [-0.0043, -0.004]$ then their next return to the cross-section fall onto two segments that are close to the initial line and within the segment $z \in [-0.0043, -0.004]$. Figure 14(b) graphs these returns, showing the z-coordinates z_{out} of returns of the 600 initial conditions versus their inital z-coordinates z_{in}; the diagonal $z_{\mathrm{out}} = z_{\mathrm{in}}$ is also pictured. This figure suggests that the return map near the line segment can be approximated by a rank-one map with two segments of slopes close to one, separated by a steep segment for initial values $z_{\mathrm{in}} \approx -0.004055$. The return map increases z on the
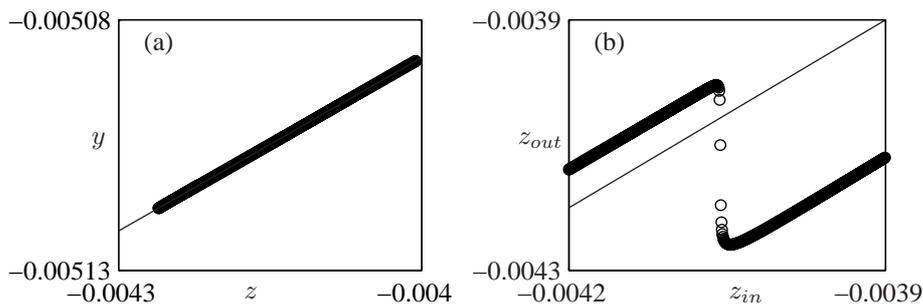
FIG. 14. *Return map of system (3.6) with* $(\nu, a, b, c, \varepsilon) = (0.0003, 0, -0.005, 0, 0.01)$ *to the section* $x = 0$. *Panel (a) shows that the return is almost one dimensional along a line that is approximately given by* $y = 0.1153\, z -$ *0.004626. The z-coordinates of the returns for initial conditions along this line with* $z \in [-0.0043, -0.004]$ *are plotted versus their initial z-values in panel (b).*

left "branch" of this map and decreases z on the right branch. This is the behavior described above since larger values of z correspond to SAOs, the smaller values to LAOs. Trajectories that do not hit the steep section of the map go back and forth repeatedly between the two branches. As ν varies, the "shape" of the return map remains qualitatively the same: the two branches still have slopes close to one, but their off-set from the diagonal varies. Approximately for $\nu < 0.00013$, the image of the right branch, representing SAOs, maps to itself, while for $\nu > 0.00034$, the image of the left branch maps to itself, and the system only has a large periodic relaxation oscillation with no SAOs. In the range of ν where MMOs do exist, *kneading theory* for one-dimensional maps [38] can be applied to the numerically generated return maps to predict the signatures of the MMOs.

Further insight into the steep segment of the return map at $z = z_{\text{in}} \approx -0.004055$ comes from computing intersections of the attracting and repelling slow manifolds. We computed forward trajectories from initial conditions on the attracting sheet (with $x < -\frac{2}{3}$) and backward trajectories from initial conditions on the repelling sheet of the critical manifold to their intersection with the cross-section $\{x = 0\}$. Since the trajectories quickly converge to the attracting and repelling slow manifolds, their intersections with $\{x = 0\}$ give a good approximation of the intersection curves of the slow manifolds with $\{x = 0\}$. These two intersection curves have one point in common, which is approximately $(y, z) = (-0.0050941, -0.0040564)$. Hence, this point lies in the region that gives rise to the steep segment shown in Figure 14(b). By definition, the intersection of the attracting and repelling slow manifolds is a maximal canard. Initial conditions on the cross-section $\{x = 0\}$ to one side of the repelling manifold result in SAOs while trajectories on the other side result in fast jumps to the other sheet of the attracting slow manifold (with $x > 0$). Thus, we have confirmed numerically that canard orbits separate the two branches of the return map displayed in Figure 14(b); compare also with Figure 7(a), which illustrates that the one-dimensional return map calculated near a folded node has several steep sections that correspond to the primary strong canard and the maximal secondary canards of the problem.

3.4. MMOs due to dynamic Hopf bifurcation and tourbillion. Recall from Section 3.3 that the abrupt transitions between SAOs and LAOs in system (3.7) are a consequence of the three-time-scale structure, which allows us to view the system as having two fast variables and only one slow variable. Such a system with two or more fast variables may have a Hopf bifurcation in the layer equations. We now consider this situation, and assume that a pair of complex eigenvalues of the layer equations cross the imaginary axis as one follows a

25

trajectory of the reduced system. When $\varepsilon \neq 0$ one observes a slow motion or drift of trajectories through the region near the Hopf bifurcation in the layer equations. Due to the complex eigenvalues in the fast directions, trajectories spiral around the slow manifold, which gives rise to oscillations. The amplitude of such an oscillation initially decreases (while the real part of the complex eigenvalues is negative) and then increase again (after the real part becomes positive). We refer to this situation as a *dynamic Hopf bifurcation*. Our primary goal is to determine when MMOs have SAOs that are associated with a dynamic Hopf bifurcation. Note that, unlike in systems with a single fast variable, this type of SAO is neither associated with a folded singularity of the critical manifold nor with a (singular) Hopf bifurcation of the system for $\varepsilon \neq 0$.

A well-known example of a dynamic Hopf bifurcation is the phenomenon of delayed Hopf bifurcation. For simplicity, we discuss it here for a system with one slow and two fast variables, the lowest dimensions possible. Consider a segment L on the one-dimensional critical manifold S along which the layer equations undergo a Hopf bifurcation. That means that the linearization of the layer equations along L has a pair of complex eigenvalues $\alpha \pm i\beta$ that cross the imaginary axis transversally. In the case of a supercritical Hopf bifurcation, a one-parameter family of attracting periodic orbits of the layer equations, parameterized by the slow variable, emanates from the point $L_0 \in L$ where $\alpha = 0$. If a trajectory $u(t)$ of the full system comes close to L near a point $L_u \in L$ that lies at a distance $\delta = |L_u - L_0| = O(1)$ from L_0, then $u(t)$ will come exponentially close to L on the slow time scale. The layer equations undergo a Hopf bifurcation, but, in analytic systems, $u(t)$ remains close to L for an $O(1)$-distance *after* the Hopf bifurcation has occurred [168]. This *delay* happens because it takes an $O(1)$ time for $u(t)$ to be repelled away from L. In particular, $u(t)$ does not immediately follow the periodic orbits of the layer equations emanating from L_0. The slow-fast analysis identifies a definite "jump" point (called a *buffer point*) at which $u(t)$ leaves L and approaches the periodic orbits, if it has not done so earlier. There are SAOs along L in a delayed Hopf bifurcation, but they are exponentially small near L_0 and the jump from L to the periodic orbits may occur within a single period of the SAOs. Thus, SAOs near a delayed Hopf bifurcation are typically so small that they are unobservable in practical examples. This situation is reminiscent of MMOs associated with folded nodes with $\delta = O(1)$. More specifically, Theorem 3.2 predicts maximal 1^{k+1} MMO signatures but, due to strong contraction toward the primary weak canard γ_w on $S_{a,\varepsilon}$, only the final rotation is actually observed; see Figure 7(b4).

In a number of examples, such as those in Sections 6 and 7, one actually observes MMOs with SAOs near a dynamic Hopf bifurcation whose amplitudes remain observably large. We adopt the term *tourbillion* from Wallet [232] to describe the trajectories passing through a dynamic Hopf bifurcation with oscillations whose amplitude remains above an observable threshold. We discuss the tourbillion and how it gives rise to MMOs also in systems with one slow and two fast variables. Consider the model system

$$\begin{cases} \dot{x} &= -y + z\,x, \\ \dot{y} &= x + z\,y, \\ \dot{z} &= \varepsilon, \end{cases} \qquad (3.9)$$

that is obtained by linearization of the layer equations for a dynamic Hopf bifurcation. This equation is separable in polar coordinates, yielding $\dot{r} = \varepsilon\, t\, r$ for trajectories that have initial conditions in the plane $\{z = 0\}$. Hence, the general solution is $r(t) = r(0)\exp(\varepsilon\, t^2/2)$, which means that the amplitude of a solution decreases for $z < 0$ and then increases for $z > 0$. We conclude that $\frac{r(1/\sqrt{\varepsilon})}{r(0)} = \exp(\frac{1}{2})$ and that the oscillations have almost constant amplitude over a time interval of $1/\sqrt{\varepsilon}$. If the r coordinate of a trajectory decreases to $r = 1$
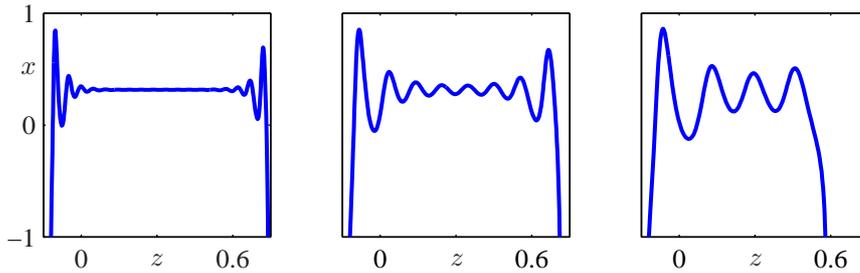
FIG. 15. *Time series of the x-coordinate of a trajectory of* (3.10) *with initial point* $(x, y, z) = (-1, 0.8, -0.12)$. *Panels (a)–(c) are for* $\lambda = 0.1$ *and for* $\varepsilon = 0.006$, $\varepsilon = 0.012$ *and* $\varepsilon = 0.02$, *respectively.*

at a value of z that is $O(\sqrt{\varepsilon})$, then the minimum amplitude of the oscillations associated with the dynamic Hopf bifurcation will still be observable. The amplitudes of these oscillations and the coupling of ε with the distance of approach to the dynamic Hopf point characterize the tourbillion regime and distinguishes it from a delayed Hopf bifurcation. In a delayed Hopf bifurcation, a trajectory approaches the slow manifold at distance $O(1)$ from the dynamic Hopf point, while in a tourbillion, the approach to the slow manifold occurs within $O(\sqrt{\varepsilon})$ of the layer containing the dynamic Hopf point. When ε is fixed in a system, the distinction between a delayed Hopf point and a tourbillion becomes blurred, but the distinction is clear in many examples.

The system (3.9) describes SAOs with distinctly nonzero amplitudes locally near the point where the dynamic Hopf bifurcation occurs in the layer not account for characteristic abrupt transitions at the beginning and end of an SAO epoch within an MMO, such as those in Sections 6 and 7, because these transitions depend upon mechanisms that are not part of the local analysis of system (3.9). There is as yet no comprehensive study of possible geometric mechanisms that determine the sudden start and the end of a section of SAOs arising from a tourbillion. This paper largely avoids this issue and concentrates on local mechanisms for generating the SAOs of MMOs. Nevertheless, the following example illustrates one mechanism for an abrupt jump away from SAOs of a tourbillion. Consider a "dynamic" section through the unfolding of the codimension-two Bogdanov-Takens bifurcation [88], defined as

$$\begin{cases} \dot{x} &= y, \\ \dot{y} &= \lambda + z\,y - x^2 - x\,y, \\ \dot{z} &= \varepsilon. \end{cases} \qquad (3.10)$$

As before, we regard z as a slowly varying parameter. For $\lambda > 0$ and $\varepsilon = 0$, the system has two straight lines of equilibria defined by $x = \pm\sqrt{\lambda}$ and $y = 0$. A supercritical Hopf bifurcation occurs along the line of equilibria with $x > 0$. The family of periodic orbits born at this bifurcation terminates at a homoclinic orbit. Moreover, there is always a bounded region of the (x, y)-plane in which oscillations around the equilibrium occur; this is the tourbillion region. The line of (saddle) equilibria with $x < 0$ of the layer equations perturbs to a Fenichel manifold of saddle type and its stable and unstable manifolds guide the entrance and exit to the tourbillion in this example. As we have seen, the number of oscillations and their minimum amplitude is determined both by the magnitude of the initial condition and of ε. This is illustrated in Figure 15 with trajectories of system (3.10) for $\lambda = 0.1$ and different values of ε — all starting from the initial condition $(x, y, z) = (-1, 0.8, -0.12)$ that lies outside the tourbillion region. Note that x and y are $O(1)$ quantities, and so the condition for a tourbillion is that $|z|$ is of order $\sqrt{\varepsilon}$. In Figure 15(a) for $\varepsilon = 0.006$ we do not find a tourbillion but

27

observe oscillations that decay rapidly, are very small for a while and then grow rapidly again before the trajectory jumps away. In panel (b) for $\varepsilon = 0.012$, on the other hand, the oscillations decay and then grow more gradually and they remain of observable size throughout. We conclude that ε is now just about large enough to speak of a tourbillion region, passage through which results in seven SAOs before the jump occurs. For even larger values of ε the same initial condition results in oscillations that maintain an almost constant amplitiude; see Figure 15(c) for $\varepsilon = 0.02$. Observe that, owing to the faster drift through the region near the Hopf bifurcation in the layer system, we now find only four SAOs before the trajectory jumps away.

It is interesting to compare the SAOs associated with a tourbillion with those occurring near a folded node or near a singular Hopf bifurcation. One difference is that the period of the oscillations is $O(\varepsilon)$ (slow time) for the tourbillion, while it is $O(\sqrt{\varepsilon})$ for the other two cases. In each of the cases, the data that determines the number of SAOs is slightly different. For the folded node, the eigenvalue ration μ determines the number of rotational sectors, and the distance of the global return to the weak canard relative to the singular perturbation parameter determines which rotational sector a trajectory enters. For the singular Hopf bifurcation, the distance of the global return to the stable manifold of the saddle-focus equilibrium sets the minimum amplitude and duration of the SAOs. For a tourbillion, the number of SAOs is governed by the singular perturbation parameter and the distance of the global return to the delayed Hopf bifurcation point. Moreover, the termination of the SAOs for a tourbillion depends upon either a global mechanism or an arbitrary threshold for the amplitude of SAOs. In contrast, the oscillations of a folded node end "on their own," while the intersections of the unstable manifold of the equilibrium and the repelling slow manifold typically limit the amplitude of SAOs near a singular Hopf bifurcation.

3.5. Summary of local mechanisms for SAOs. We now summarize the main results of this review section on the local mechanisms that give rise to MMOs. For systems with a single fast variable, the local mechanisms responsible for SAOs must involve a mixture of the two time scales. We distinguish three regions near folded nodes and folded saddle-nodes that yield MMOs:

1. *Folded Nodes:* If the parameters satisfy suitable order conditions ($\nu = O(1)$) so that no equilibrium of the full system is near the folded node then the theory of Section 3.1 applies and SAOs are due to the *twisting of slow manifolds*.
2. *Singular Hopf:* As is shown in the Section 3.2, the dynamics near a singular Hopf bifurcation ($\nu = O(\varepsilon)$) tends to be quite complicated. SAOs occur when the trajectory follows the *unstable manifold of a saddle-focus*.
3. *Transition Regime:* The folded-node and singular-Hopf regimes are separated by a transition regime with intermediate values of $\nu = O(\sqrt{\varepsilon})$. Extensions of the folded node theory have been developed in [143]; note that the parameter μ in [143] not only represents the eigenvalue ratio but also describes the distance of the equilibrium to the folded node in a blown-up system. In this transition regime, it is possible for the SAOs to pass through the rotational sectors of the folded node *as well as* spiral along the unstable manifold of the saddle-focus equilibrium.

In systems with at least two fast variables the tourbillion provides a different local mechanism that generates SAOs. Here, the layer equations have complex eigenvalues and the SAOs are aligned with the fast directions of the system. Little systematic study of the tourbillion as a mechanism that generates MMOs has been carried out, and the theory remains fragmentary.

Finally, three-dimensional systems with three time scales can exhibit all of the mechanisms discussed in this section. Namely a three-time-scale system may be considered as

having two slow variables, in which case the folded-node and singular-Hopf mechanisms may be found, or, alternatively, as having two fast variables, which allows for the possibility of a tourbillion.

The following sections are case studies that illustrate these different local mechanisms for MMOs:

- The *Koper model* in Section 4 is a three-dimensional slow-fast system with a folded node and a supercritical singular Hopf bifurcation.
- The three-dimensional *reduced Hodgkin–Huxley model* in Section 5 also features a folded node, but has a subcritical singular Hopf bifurcation.
- The four-dimensional *Olsen model of the peroxidase-oxidase reaction* in Section 6 displays MMOs associated with a tourbillion.
- The *Showalter–Noyes–Bar-Eli model* in Section 7 is a seven-dimensional system that exhibits MMOs. The global mechanism that organizes these MMOs is unknown, but we show here that their SAOs are due to a tourbillion.

4. MMOs in the Koper model of chemical reactors. Our first case study is a system introduced by Koper [122]. We use it to illustrate how MMOs arise near a folded node and near a (supercritical) singular Hopf bifurcation in a specific model equation. The equations of the Koper model are

$$
\begin{cases}
\varepsilon_1 \dot{x} &= k\, y - x^3 + 3\, x - \lambda, \\
\dot{y} &= x - 2\, y + z, \\
\dot{z} &= \varepsilon_2\, (y - z),
\end{cases}
\tag{4.1}
$$

where λ and k are parameters. Koper studied this three-dimensional idealized model of chemical reactions with MMOs. While this example is well known, we revisit its analysis and enhance it by using the recently developed theory outlined in the previous sections. When ε_1 and ε_2 are both small, system (4.1) has three time scales; when only ε_1 is small, it is a slow-fast system with two slow variables y and z and one fast variable x. We note that a two-dimensional variant of (4.1) was first studied by Boissonade and De Kepper [26] in their efforts to understand bistability and oscillations of chemical systems. The first analysis of MMOs in the three-dimensional extended model was carried out by Koper who explained the MMOs by invoking the presence of a Shil′nikov homoclinic bifurcation.

As mentioned in Section 3.2, the Koper model (4.1) is a rescaled subfamily of the cubic normal form (3.6) for the singular Hopf bifurcation. To see this, replace (x, y, z) in system (4.1) by (u, v, w) and consider the affine coordinate change

$$
x = \frac{u - 1}{3}, \quad y = \frac{k\, v - \lambda + 2}{27}, \quad z = \frac{2\, v - w - 1}{3}.
$$

Now also scale time by the factor $\frac{-k}{9}$, where we assume that $k < 0$. Then (4.1) becomes (3.6) with $\varepsilon = -k\, \varepsilon_1 / 81$, $a = 18/k$, $b = 81\, \varepsilon_2 / k^2$, $c = -9\, (\varepsilon_2 + 2)/k$ and $\nu = (3\, \varepsilon_2\, \lambda - 6\, \varepsilon_2 - 3\, k\, \varepsilon_2 / k^2)$. Note that the coefficients of the normal form satisfy

$$
2\, b - a\, c + a^2 = 0,
$$

which means that the Koper model (4.1) is only equivalent to a subfamily of the singular-Hopf normal form (3.6). However, (4.1) still has a folded node and a singular Hopf bifurcation in certain parameter regimes.

Let us first analyze the parameter regimes where SAOs are organized by a folded node.

29